1   **Single extracellular vesicle analysis in human amniotic fluid shows evidence of**

2   **phenotype alterations in preeclampsia**

3   Natalia Gebara[1], Julia Scheel[2], Renata Skovronova[1], Cristina Grange[3], Luca Marozio[4],

4   Shailendra Gupta[2], Veronica Giorgione[5], Federico Caicci[6], Chiara Benedetto[4], Asma Khalil[5,7],

5   Benedetta Bussolati[1*]

6   1. Department of Molecular Biotechnology and Health Sciences, University of Turin, Italy.

7   2. Department of Systems Biology and Bioinformatics, University of Rostock, Germany.

8   3. Department of Medical Sciences, University of Turin, Turin, Italy.

9   4. Department of Surgical Sciences, Obstetrics and Gynecology, University of Turin, Italy.

10   5. Vascular Biology Research Centre, Molecular and Clinical Sciences Research Institute, St
11   George's University of London, UK

12   6. DiBio Imaging facility, University of Padua, Italy.

13   7. Fetal Medicine Unit, St George's University Hospitals NHS Foundation Trust, St George's
14   University of London, UK.

15
16
17   ****Corresponding Author:** Benedetta Bussolati, Molecular Biotechnology Center, University

18   of Turin, via Nizza 52, 10126 Turin, Italy. Fax 011-6331184, Tel. 011-6706453, e-mail:

19   benedetta.bussolati@unito.it

20

21   **Running Title:** Amniotic fluid-derived EVs

22   **Disclosure:** The authors declare no conflict of interest.

1

Abstract

Amniotic fluid surrounding the developing fetus is a complex biological fluid rich in metabolically active bio-factors. The presence of extracellular vesicles (EVs) in amniotic fluid has been mainly related to fetal urine. We here characterized EVs from term amniotic fluid in terms of surface marker expression using different orthogonal techniques. EVs appeared to be a heterogeneous population expressing markers of renal, placental, epithelial and stem cells. Moreover, we compared amniotic fluid EVs from normal pregnancies with those of preeclampsia, a hypertensive disorder affecting up to 8% of pregnancies worldwide. An increase of CD105 (endoglin) expressing EVs was observed in preeclamptic amniotic fluid by bead-based cytofluorimetric analysis, and further confirmed using a chip-based analysis. HLA-G, a typical placental marker, was not co-expressed by the majority of CD105$^+$ EVs, suggesting their origin from amniotic fluid cells. At a functional level, preeclampsia-derived EVs, but not normal pregnancy EVs, showed an antiangiogenic effect, possibly due to the decoy effect of endoglin. In addition, several miRNAs were differentially expressed in preeclampsia-derived EVs and directly related to the modulation of angiogenesis and trophoblast function. Our results provide a characterization of term amniotic fluid-EVs, supporting their origin from fetal and placental cells. In preeclampsia, the observed antiangiogenic characteristics of amniotic fluid-EVs may reflect the hypoxic and antiangiogenic microenvironment and could possibly impact on the developing fetus or on the surrounding fetal membranes.

Key-words: extracellular vesicles, exosomes, amniotic fluid, placenta, pregnancy disorders, angiogenesis, soluble endoglin.

49 **Introduction**

50 Amniotic fluid is a complex biological fluid surrounding the developing fetus and in close

51 proximity to the placenta (Underwood, Gilbert and Sherman, 2005). Its composition, after fetal

52 skin keratinization, mainly consists of fetal cardiovascular, renal, pulmonary, and endothelial

53 secretions (Roubelakis, Trohatou and Anagnou, 2012). Amniotic fluid has a relevant role in

54 fetal physiology; it not only acts as a protective cushion to mechanical injury but also contains

55 a plethora of active factors, including nutrients, growth and antimicrobial factors, cells and

56 extracellular vesicles (EVs) (Underwood, Gilbert and Sherman, 2005).

57 EVs are a highly heterogeneous population of small particles enclosed in a lipid bilayer,

58 released by almost all cell types, and involved in cell-to-cell signalling. In pregnancy, EVs are

59 essential for diverse physiological and pathological processes (Jankovičová *et al.*, 2020) and

60 may play a role in angiogenesis and successful fetal development (Gebara *et al.*, 2021). The

61 role of EVs derived from placental trophoblasts has been studied extensively, as they are

62 continuously released into the maternal bloodstream and play a crucial role in regulating the

63 maternal immune response and pregnancy adaptation (Nair and Salomon, 2018). At variance,

64 the profile and function of EVs present in amniotic fluid have been poorly investigated, as their

65 characteristics have been mainly attributed to fetal urine production (Keller *et al.,* 2007).

66 Indeed, previous studies showed that a large proportion of EVs within the amniotic fluid

67 express typical renal markers, such as aquaporin-2 and CD24, demonstrating their fetal urine

68 origin (Keller *et al.,* 2007). However, multiple cells may release EVs into the amniotic fluid,

69 including the amnion, placental tissues and fetal cells (Dixon *et al.,* 2018; McMaster *et al.,*

70 1998). Interestingly, isolated amniotic epithelial or stem cells in culture were shown to release

71 EVs with trophic, immunomodulating and anti-inflammatory functions (Balbi *et al.,* 2017;

72 Sedrakyan *et al.,* 2017). It is therefore conceivable that EVs released from those cells are also

73 present in the amniotic fluid. Moreover, a recent trial reported the safe administration of a

74 pharmaceutical product, including term amniotic fluid-EVs, against the COVID-19 related

75 cytokine storm (Mitrani *et al.,* 2021). The analysis and characterization of amniotic fluid EVs

76 is therefore of interest.

77 Preeclampsia is a complex pregnancy disorder characterized by new-onset hypertension with

78 associated maternal organ dysfunction, including impaired liver function, renal damage

79 (significant proteinuria, oligoanuria, increased creatinine), low platelets, haemolysis, decreased

80 sPO_2 or pulmonary edema, or visual and cerebral disturbances (Brown *et al.*, 2018).

81 Preeclampsia affects up to 8% of pregnancies world-wide (Duley, 2009) and causes significant

82 maternal and perinatal morbidity and mortality, as well as long-term complications (Amaral *et*

83 *al.*, 2015). Abnormal placentation and insufficient trophoblast invasion are considered the main

84 causes of preeclampsia (Kaufmann, Black and Huppertz, 2003), leading to the release of

85 antiangiogenic factors that subsequently promote maternal endothelial dysfunction (Staff *et al.*,

86 2007). Several studies highlighted the presence of altered EVs in the maternal circulation of

87 preeclamptic women and their possible contribution to endothelial dysfunction (Escudero *et*

88 *al.*, 2016). Interestingly, EVs carrying antiangiogenic factors, such as soluble vascular

89 endothelial growth factor receptor 1 (sFlt-1) and soluble endoglin, were found at high levels in

90 the maternal circulation and were shown to be released by placental explants (Tannetta *et al.*,

91 2013; Chang *et al.*, 2018; Nair *et al.*, 2021). Therefore, it is of interest to evaluate whether

92 amniotic fluid EVs in preeclamptic pregnancies might have phenotypic or functional

93 differences with respect to those of normal pregnancies.

94 In the present study, we aimed to characterize amniotic fluid-derived EVs from term normal

95 and preeclamptic pregnancies. Surface marker expression was analyzed at a single-EV level

96 using different techniques, such as super-resolution microscopy, ExoView array and bead-

4

97   based cytofluorimetric analysis. In addition, their differential microRNA (miRNA) profile and

98   angiogenic properties were investigated.

99

100   **Materials and methods**

101

102   **Collection of amniotic fluid**: Amniotic fluid samples (40 from normal pregnancies and 7 from

103   preeclamptic pregnancies) were collected during caesarean delivery in the Department of

104   Surgical Sciences at the University of Turin, after approval by the Ethics Review Board of the

105   Health and Science City of Turin, (Città della Salute e della Scienza di Torino, protocol N°

106   0079734, CS2/320) and at the Maternity Department of St George's University Hospital in

107   London, after approval by the Local Ethics Committee (19/LO/0794) (Table 1). All patients

108   provided preoperative written informed consent. The fluid was collected by sterile acupuncture

109   after myometrial incision, before the incision of the amniotic membranes. Three of the

110   preeclamptic patients (n=7) were affected by comorbidities, including fetal growth restriction,

111   type two diabetes, and systemic lupus erythematosus. Further clinical information about

112   preeclamptic patients can be found in Table 2.

113   *Table 1. Clinical information showing the mean ± SD of gestational age, maternal age at*
114   *delivery and the volume of the amniotic fluid obtained from normal and preeclamptic*
115   *pregnancies.*

	Normotensive pregnancies (n=40)	Preeclampsia (n=7)
Gestational age (weeks)	37.9±1.8	36.1±2.6
Maternal age (years)	35.7±5.2	32.8±6.7
Amniotic fluid volume (ml)	19.9±7.8	18.4±11.3

116

117

118

5

119 **Table 2.** *Clinical information on individual preeclamptic patients showing the gestational age,*
120 *maternal age at delivery, week of preeclampsia diagnosis, sFlt-1/PIGF ratio, other*
121 *pathologies, treatment, and additional relevant information. PIGF:Placental growth factor.*

	Age of gestation (weeks+days)	Maternal age (years)	Preeclampsia diagnosis (weeks)	sFlt-1/PIGF ratio	Other pathologies	Treatments	Other
1	36+1	42	36	280	-	Betamethasone Nifedipine	Assisted reproduction techniques
2	32+1	32	31	531	-	Betamethasone Nifedipine MgSO₄	Fetal growth restriction
3	39+2	22	36	42	-	-	-
4	36+6	39	35	-	Chronic hypertension, systemic lupus erythematosus	Methyldopa, Nifedipine, Hydroxychloroquine, Aspirin, Low Molecular Weight Heparin	-
5	38+2	28	36	-	Type 2 diabetes	Metformin, Insulin	-
6	36+1	35	36	-	-	Labetalol, Nifedipine	Fetal growth restriction
7	36+2	33	33	-	-	Labetalol, Nifedipine, Metformin, Insulin	-

122

123 **Isolation and culture of term amniotic fluid mesenchymal stromal cells (AFSCs)**: Term

124 AFSCs were previously obtained and characterized, as described (Iampietro *et al.*, 2020).

125 Briefly, amniotic fluid was transferred into a sterile 50 mL falcon and centrifuged at 500 g for

126 10 minutes at room temperature. The cell pellet was resuspended in α-MEM Medium

127 (Gibco/BRR, ThermoFisher, MA, USA) supplemented with 20% Chang Medium B (Irvine

128 Scientific, Santa Ana, California, USA) and 2% Chang Medium C (Irvine Scientific), 20%

129 Fetal Calf Serum (Invitrogen, Carlsbad, CA, USA), 50 IU/mL penicillin, 50 g/mL

130 streptomycin, 5mM glutamine (all from Sigma-Aldrich, St. Louis, MO, USA). The cells were

131 placed into a T25 flask, incubated at 37°C on 5% CO_2 until the cells formed clusters (1-2

132 weeks). Afterwards, the medium was replaced twice a week until the cells reached confluency.

6

133 Under these culture conditions, AFSCs expressed typical mesenchymal surface markers and

134 differentiation properties, as previously described (Iampietro *et al.*, 2020).

135 **EV Isolation from amniotic fluid:** Amniotic fluid samples were diluted in PBS up to a volume

136 of 20 ml and subjected to differential centrifugations. For the isolation of cells, samples

137 underwent a 5 min centrifugation at 300 x g, at room temperature. A second centrifugation of

138 10 min was performed at 500 x g, at room temperature, for removal of debris. The supernatant

139 was then passed through a cell sieve and underwent a 30 min ultracentrifugation (70 Ti rotor,

140 Beckman Coulter, CA, USA) at 10,000 x g, at 4°C. The resulting pellet was discarded, and the

141 supernatant was further centrifuged for 2 h at 100,000 x g at 4°C. The final step included

142 resuspension of EV pellets in 1 ml 1% DMSO/PBS and additional filtration through a 0.22 µm

143 filter. The recovered EVs were stored at -80°C.

144 **EV Isolation from AFSCs:** The term AFSCs were grown to 70-80% confluency, washed twice

145 with PBS and placed in serum free RPMI medium overnight. After 16 h of incubation, the

146 RPMI medium was recovered and centrifuged at 300 x g for 5 min, 10,000 x g for 30 min,

147 followed by ultracentrifugation at 100,000 x g for 2 h at 4°C. The EV pellet was resuspended

148 in 1% DMSO/PBS and stored at -80°C.

149 **Smart SEC purification:** Size-exclusion chromatography was applied to samples destined for

150 miRNA arrays and ExoView analysis. Following differential ultracentrifugation, EV pellets

151 were resuspended in 100 µl of PBS and applied to Smart SEC columns (SSEC100A-1,

152 BioNova, Madrid, Spain). The samples were then processed as recommended by the

153 manufacturer's protocol.

154 **Transmission electron microscopy**: One drop of PBS (about 25 µl) containing EV at 5.8×10^8

155 was placed on a 400-mesh holey film grid; after staining with 2% uranyl acetate (for 2 minutes)

156 the sample was observed with a Tecnai G2 transmission electron microscope (FEI Company,

7

157   Hillsboro, OR, USA) operating at 100 kV. Images were captured with a Veleta digital camera

158   (Olympus Soft Imaging System, Tokyo, Japan).

159   **NanoSight analysis:** The size and concentration of EVs was determined by nanoparticle

160   tracing analysis (NTA) performed by NanoSight LM10 system (Malvern Panalytical, Malvern,

161   UK). Each vesicle sample was diluted (1:100) in PBS (filtered with a 0.22 µm filter). For each

162   sample, a syringe pump flow of 30 was applied. Three videos of 60 seconds each were recorded

163   and analyzed, calculating an average number of EV size and concentration (particles/ml). All

164   samples were characterized with NTA 3.2 analytical software. The NTA settings were kept

165   constant between the samples.

166   **Super-resolution microscopy**: Super-resolution microscopy pictures of EVs were obtained

167   using a temperature-controlled Nanoimager S Mark II microscope from ONI (Oxford

168   Nanoimaging, Oxford, UK) equipped with a 100x, 1.4NA oil immersion objective, an XYZ

169   closed-loop piezo 736 stage, and 405 nm/150 mW, 473 nm/1 W, 560 nm/1 W, 640 nm/1 W

170   lasers and dual or triple emission channels split at 640 / and 555 nm. For sample preparation,

171   10 µl of 0.01% Poly-L-Lysine (Sigma-Aldrich, St. Louis, MO, USA) was placed on high-

172   precision coverslips previously cleaned in a sonication bath twice in dH_2O and once in KOH,

173   in silicon gasket (Grace Bio-Labs, Sigma-Aldrich). The coverslips were placed at 37°C in a

174   humidifying chamber for two hours. Excess of Poly-L-Lysine was removed. 1 µl of EVs

175    $(1x10^{10})$ resuspended in 9 µl of blocking solution (PBS-5% Bovine Serum Albumin) was

176   pipetted into a previously coated well to attach overnight at +4°C. The next day, the sample

177   was removed, and 10 µl of blocking solution was added into the wells for 30 min. Then, 2.5 µg

178   of purified mouse anti-CD9 conjugated with Atto 488 dye (ONI), anti-CD63 antibodies (SC-

179   5275, SC-31234, Santa Cruz, CA, USA) conjugated with Alexa Fluor 647 dye, HLA-G

180   antibody (SC-21799, Santa Cruz) conjugated with Alexa Fluor 555 dye, were prepared using

8

181   the Apex Antibody Labelling Kit (Invitrogen) according to the manufacturer's protocol. One

182   µl of each antibody was added into the blocking buffer at a final dilution of 1:10. Samples were

183   incubated in the dark at +4°C. The day after, samples were washed twice with PBS, and 10 µl

184   of the mixed ONI B-Cubed Imaging Buffer (Alfatest, Rome, Italy) was added for amplification

185   of the EV signalling. Before each imaging session, bead slide calibration was performed for

186   aligning the channels, to achieve a channel mapping precision smaller than 12 nm. Images were

187   taken in dSTORM mode using 30% laser power for the 647 nm, 50% laser power for the 488

188   nm laser, and 30% for the 555 channel. Two-channels (647 and 555) dSTORM data (5000

189   frames per channel) or three-channels (2000 frames per channel) (647, 555 and 488) were

190   acquired sequentially at 30 Hz (Hertz) in total reflection fluorescence (TIRF) mode. Single-

191   molecule data was filtered using NimOS software (v.1.18.3, ONI) based on the point spread

192   function shape, photon count and localization precision to minimize background noise and

193   remove low-precision and non-specific colocalization. Data has been processed with the

194   Collaborative Discovery (CODI) online analysis platform www.alto.codi.bio from ONI and the

195   drift correction pipeline version 0.2.3 was used. Clustering analysis was performed on

196   localizations and BD clustering constrained parameters were defined (photon count 300-max,

197   sigma 0-200 nm, p-value 0-1, localization precision 0-20 nm). Colocalization was defined by

198   a minimum number of localizations for each fluorophore/protein within a distance of 100 nm

199   or distance used from the centroid position of a cluster.

200   **Western Blot:** For protein analysis, EVs were lysed at 4°C for 30 min in RIPA buffer (20 nM

201   Tris-HCl, 150 nM NaCl, 1% deoxycholate, 0.1% SDS, 1% Triton X-100, pH 7.8)

202   supplemented with a cocktail of protease and phosphatase inhibitors and PMSF (Sigma-

203   Aldrich). For protein concentrations of less than 2 mg/ml, a precipitation step was applied. The

204   pellet was resuspended in Laemmli Buffer and the sample was loaded onto the gel. As

205   determined by the Bradford method, aliquots of the cell lysates containing 10-15 µg of proteins

9

206 were run on 4-20% acrylamide gel SDS-PAGE under reducing conditions. The transfer of

207 proteins onto a PVDF membrane was performed using the iBlot™ Dry Blotting System (Life

208 Technology). Primary antibodies used were: CD81 at 1:200 (SC-31234), CD63 at 1:200 (SC-

209 5275), HLA-G at 1:200 (SC-21799), (all from Santa Cruz), CD105 at 1:1000 (362-820, Ancell)

210 and at 1:2000 calreticulin (2891S, Cell Signaling Technology, Danvers, MA, USA).

211 Chemiluminescent signal was detected using the ECL substrate (Bio-Rad), and bands were

212 detected by the ChemiDoc system (Bio-rad, Hercules, CA, USA).

213 **MACSPlex:** EV samples were tested with a bead-based multiplex analysis (MACSPlex

214 exosome kit, human, Miltenyi Biotec, Bergisch Galdbach, Germany). EV samples were diluted

215 with MACSPlex buffer to a final volume of 120 µl with 5.8×10^8 EVs per sample. Fifteen µl of

216 MACSPlex Exosome Capture Beads and 15 µl of the antibody cocktail composed of APC

217 conjugated CD9, CD63 and CD81 were added to the buffer containing EVs and incubated on

218 an orbital shaker at 12 rpm for 1 hour protected from light, at room temperature. After the

219 incubation, 1 ml of MACSPlex buffer was added and the samples were centrifuged at 3,000 g

220 for 5 min. After a second wash, the samples were incubated for a further 15 min on the orbital

221 shaker. Thereafter the samples were centrifuged and prepared for flow cytometry analysis.

222 Median fluorescence intensity was calculated for all 39 bead populations. The analysis of the

223 samples was performed by subtraction of the control and the fluorescence controls. For analysis

224 of AFSC-EVs, the same method was followed with the substitution of the fluorescent antibody

225 mix against tetraspanins (CD63, CD81 and CD9) with the APC labelled HLA-G antibody

226 (130111852, Miltenyi Biotec, same volume of 15 µl). This method ensured that EVs attached

227 to the Ab conjugated beads were only detected if positive for HLA-G.

228 **ExoView array:** For the analysis with the ExoView platform^TM (NanoView Biosciences,

229 Boston, MA, USA), EVs were further purified with Smart SEC columns (BioNova), and the

10

230   collected fractions were applied directly to the ExoView chips. 10-35 µl of the sample with a

231   concentration of $5x10^8$ EVs was applied to a final volume of 35 µl in the incubation solution.

232   EVs were then incubated overnight at room temperature. Immuno-fluorescence staining was

233   performed using antibodies provided by the company (0.6 µl of CD63, CD81, CD9). Alexa

234   Fluor 488 conjugated anti-CD117 (ab2164459, Abcam, Cambridge, UK), anti-Tie-2 (ab24859,

235   Abcam), anti-CD105 (362-820, Ancell) and HLA-G conjugated with Alexa Fluor 555 (SC-

236   21799, Santa Cruz) were used for detection of EV subpopulations. For all antibodies, the Apex

237   Antibody Labelling Kit was used (Invitrogen). All antibody conjugations were performed

238   according to manufacturer's protocol. Chips were analyzed using the ExoView™ R100 reader

239   using ExoView Scanner software (v 3.0). The data were analyzed using ExoView Analyzer (v

240   3.0). Two sets of ExoView chips were tested. The first set of chips were pre-spotted with

241   CD63/CD81/CD9, with addition of fluorescent antibodies CD63, CD81, CD9. The second set

242   of chips were pre-spotted with CD63/CD81/CD9 with the addition of fluorescent antibodies

243   HLA-G, CD117, Tie-2 and CD105.

244   **Angiogenesis:** Human umbilical vascular endothelial cells (HUVEC) were bought from ATCC

245   (ATCC-PCS-100-010, Manassas, VA, USA). Cells were cultured until the 6th passage in

246   complete EBM medium (Lonza, Basel, Switzerland). Cell medium was changed three times

247   per week, and cells were passaged when they reached 70-80% confluency. The cells were split

248   by washing in PBS, then applying 2 ml of 10% trypsin-EDTA and re-plated on T75 flasks

249   coated with attachment factor (S-006-100, Gibco). *In vitro* formation of capillary-like

250   structures was performed on growth factor–reduced Matrigel (356231, Corning, NY, USA).

251   HUVEC cells were mixed with EVs (1000 EVs/cell) and/or anti-CD105 Ab TRC-105 8 µg/ml

252   (TRACON Pharmaceuticals, CA, USA) and recombinant soluble CD105 (s-Endoglin, 100

253   ng/ml; C-60059, PromoKine, Heidelberg, Germany) in complete EBM medium and seeded at

254   a density of 15×10^3 cells per well on a 24-well plate. For combination of EVs with the anti-

11

255   CD105 Ab TRC-105, both components were mixed and incubated for 25 min at room

256   temperature, prior to adding them to the cell suspension. Cells were periodically observed with

257   a Nikon TE2000E inverted microscope (Nikon, Tokyo, Japan), and experimental results were

258   recorded after 16 h; 5 images were taken per well. Image analysis was performed with the

259   ImageJ software v.1.53c, using the Angiogenesis Analyzer. The data from three independent

260   experiments were expressed as the mean ± SD of tube length in arbitrary units per field.

261   **miRNA array analysis:** Total EV RNA was extracted from 3 normal and 3 preeclamptic

262   amniotic fluid samples after ultracentrifugation and SEC. All samples were processed

263   separately. RNA was extracted using *mir*Vana miRNA Isolation Kit (AM1560, ThermoFisher)

264   following the manufacturer's protocol. The RNA concentration was measured using NanoDrop

265   (NanoDrop ND-1000, ThermoFisher) and precipitated to a final concentration of 10 ng/μl. The

266   total cDNA was pre-amplified prior to miRNA quantification. Expression of 754 different

267   miRNAs was evaluated by quantitative real-time PCR using TaqMan Array MicroRNA card

268   A (v.3.0) and B (v.3.0) and according to Megaplex manufacturers protocol. All the samples

269   were run separately. Quantification was performed using a QuantStudio 12K Flex Real-Time

270   PCR System (Applied Biosystems, Waltham, MA, USA). Ct values were analyzed by

271   Expression Suite software v1.3 using global normalization. A maximum threshold of 35 was

272   applied for analysis of EVs from normal pregnancies in comparison to preeclampsia.

273   **Quantitative real-time PCR:** Validation of the miRNAs was performed by quantitative real-

274   time PCR (qRT-PCR) on 3 different amniotic fluid EV samples for normal pregnancy and

275   preeclampsia. The miRNAs were reverse-transcribed into cDNA using a High Capacity cDNA

276   reverse transcription kit (Applied Biosystems) following the manufacturer's protocol. The

277   qRT-PCR was performed using 20 miRNA primers (Supplementary Table 1) and miScript

278   SYBR Green PCR Kit (Qiagen, Hilden, Germany). RNA U6 was used as the endogenous

12

279   control. The samples were analysed using the comparative CT method. In total 20 miRNAs

280   were selected and validated, based on literature research via Pubmed interrogation with the

281   following keywords: "miRNAx" and "angiogenesis or placenta or pre-eclampsia" or

282   "miRNAx" and "angiogenesis or placenta or pre-eclampsia" and extracellular vesicles".

283   **Acquisition of PE-related miRNAs gene targets and transcription factors and network**

284   **visualization:** We obtained PE associated miRNAs based on previously mentioned

285   experiments. miRTarBase v8.0 was used to identify gene targets and extract miRNA-gene pairs

286   (Huang *et al.*, 2020). To minimize false positives, only strong-evidence miRNA-target pairs

287   were considered. Literature-curated transcription factor (TF)-miRNA pairs of deregulated

288   miRNAs were extracted from TransmiR (Tong *et al.*, 2019) miRNA, target gene, and TF

289   interaction pairs were visualized in Cytoscape v3.8.2 (Shannon *et al.*, 2003). The interactions

290   between genes and TF, and interacting genes were integrated using the Cytoscape App

291   Bisogenet v3.0.0 (Martin *et al.*, 2010).

292   **Network enrichment analysis:** The analysis of overrepresented gene ontology (GO)

293   biological process terms and pathways associated with the target genes, was performed using

294   EnrichR webtools (Chen *et al.*, 2013). Ontology and pathway GO terms with an adjusted p-

295   value <0.05 were considered significantly overrepresented. In addition, the Cytoscape App

296   BinGo was used to visualize and cluster the gene annotation terms into groups (Maere,

297   Heymans and Kuiper, 2005). BinGo results were corrected for multiple testing using

298   Benjamini-Hochberg false discovery rate correction. The KEGG, Reactome and WikiPathways

299   databases, as well as the Tissue Expression ArchS4 databases, were used to obtain specific

300   gene annotations (Ogata *et al.*, 1999; Rouillard *et al.*, 2016; Jassal *et al.*, 2020). The comparison

301   of miRNA-gene target interactions and GO biological processes to previous studies (Pillay *et*

302   *al*., 2019 and Salomon *et al.*, 2017) was performed using Cytoscape ClueGO plugin (Bindea *et*

13

303   *al.*, 2009). GO biological process function terms with an adjusted p value <0.001 after

304   Bonferroni step down correction and term fusion were considered.

305   **Synergistically working miRNAs:** MiRNAs with binding sites near each other (between 13-

306   35 nucleotides) can cooperate in target repression. We identified cooperating miRNA pairs of

307   upregulated   preeclampsia-associated   miRNAs   using   the   TriplexRNA   database

308   (https://triplexrna.org/). The results were filtered for targets involved in angiogenesis based on

309   GO terms (Lai *et al.*, 2012).

310   **Statistical tests:** All statistical analyses were performed using GraphPad Prism software (v.

311   8.00; GraphPad, CA, USA). For comparisons of each group, an unpaired Student's t-test was

312   used. FWelch's correction was performed when the variance across groups was assumed to be

313   unequal. Differences were considered significant when the p-value was <0.05. For multiple

314   comparison analyses, ANOVA with Bonferroni multicomparison post hoc test. A two-tailed *p*-

315   value <0.05 was considered statistically significant.

14

Results

Characterization of amniotic fluid-derived EVs

EVs were isolated from term amniotic fluid of 40 normal pregnancies (Table 1) by differential

ultracentrifugation followed by filtration and, for selected experiments (miRNA and ExoView

analysis), by size-exclusion chromatography. The normal pregnancy EVs (NP-EVs) were first

characterized based on their size and concentration using nanoparticle tracking analysis (Figure

1A). Homogeneous concentration and particle size were obtained among the different samples,

with a mean size of 221.8±6.2 nm. Western Blot analysis confirmed the expression of EV

specific markers (CD63, CD81) and revealed the presence of the placental maker HLA-G,

previously shown to characterize placental-derived EVs (Orozco *et al*., 2009) (Figure 1B). The

absence of the cytoplasmic marker calreticulin showed a lack of cellular contamination (Figure

1B). TEM showed heterogeneous EV populations (particles ranging from approximately 50 to

approximately 200 nm in diameter) (Figure 1C). To quantify the expression of CD63 and HLA-

G and to assess their possible colocalization, we performed super-resolution imaging of NP-

EVs using dSTORM. More than 6,000 single-EV images were acquired and analyzed.

Clustering analysis showed that the majority (around 87%) of CD63^{+} EVs also expressed HLA-

G (Figure 1D).

15
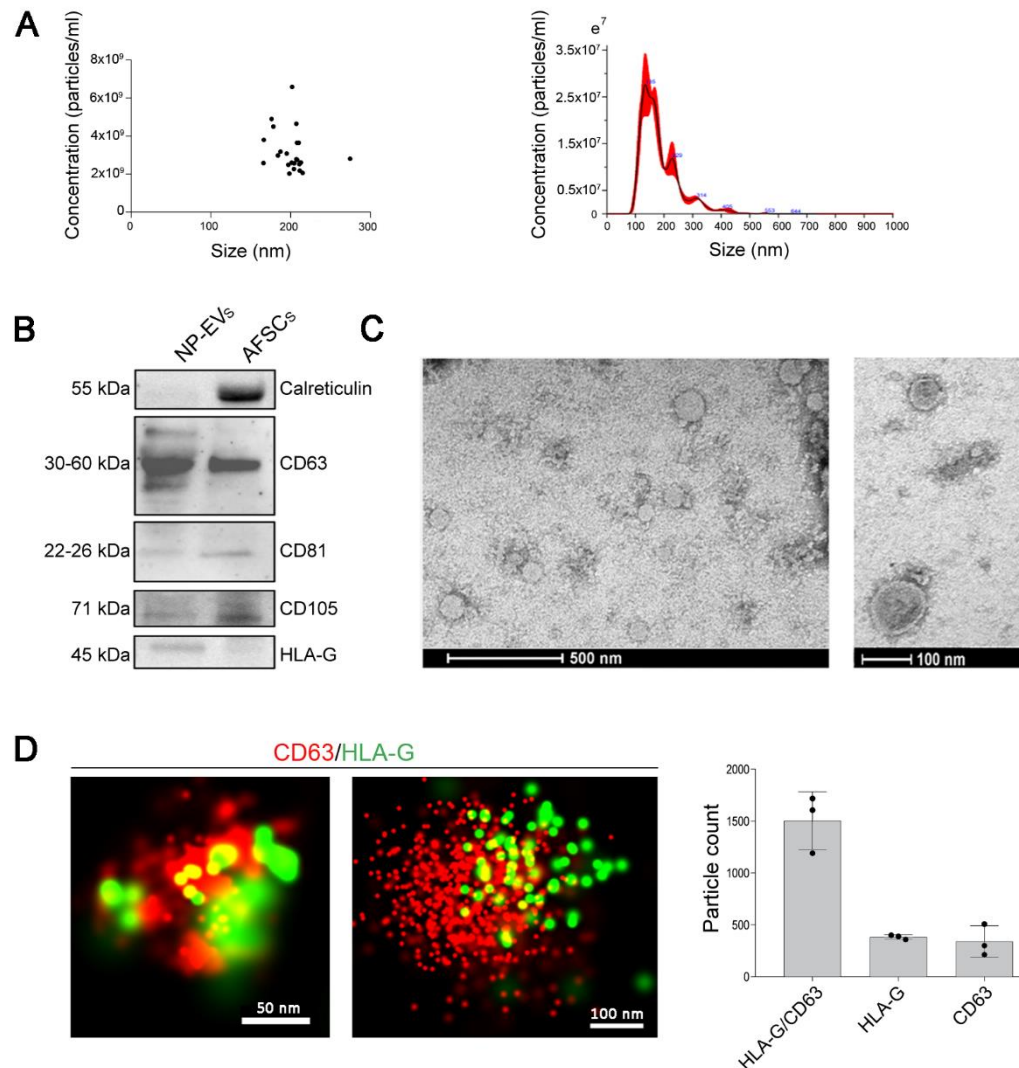
*Figure 1. **Characterization of NP-EVs**. A) Nanoparticle tracking analysis of NP-EVs (n=30) showing homogenous size and concentration. Dilution of 1:100 in PBS in 1ml was used to test the samples (left panel). A representative graph showing size distribution of a NP-EV sample (right panel). **B)** Representative Western Blot image showing the presence of CD63, CD81, CD105 and HLA-G in NP-EVs (10-15 µg proteins) and in AFSC lysate (10-15 µg proteins) and the presence of calreticulin in cell lysate only. Three different NP-EV samples were tested with similar results. **C)** Representative transmission electron microscopy images at low- and high-power fields of NP-EVs showing heterogenous EV population. **D)** Representative super-resolution microscopy images of single amniotic fluid-derived EVs expressing CD63 (red) and HLA-G (green). The number of single and double positive EVs for CD63 and HLA-G was analysed in 3 NP-EV preparations using the CODI software; the graph shows the mean ± SD of a cumulative analysis of 10 fields for each preparation, total EV number: 6,676.*

In addition, super-resolution microscopy was used to analyze the size and expression of

tetraspanin markers (CD63, CD81 and CD9) at a single-molecule level in NP-EVs (Figure 2).

The results showed that NP-EVs were a heterogeneous population with highly variable

tetraspanin expression (Figure 2E). The analysis of more than 20,000 EVs using a dedicated

16

352   software (https://alto.codi.bio/) showed that the majority of EVs were either triple positive for

353   CD63, CD81 and CD9 or double positive for CD81 and CD9, with lower fractions expressing

354   double or single tetraspanins (Figure 2E). The overall average particle size evaluated by the

355   super-resolution microscope was 121±26 nm. This measurement, based on specific EV

356   detection using tetraspanins, overlaps the results obtained by transmission electron microscopy.

357   The larger EV size detected by nanoparticle tracking analysis can be possibly explained by the

358   evaluation of the EV hydrodynamic size, under solution using this technique, in comparison

359   with the measurement of the dry radius with microscopy techniques (Montis *et al*., 2017). In

360   addition, possible artifacts including EV aggregates or non-EV particles can be detected by

361   nanoparticle tracking analysis, suggesting that it should be applied for size evaluation together

362   with other side techniques, as previously described (Skovronova *et al.*, 2021).

17
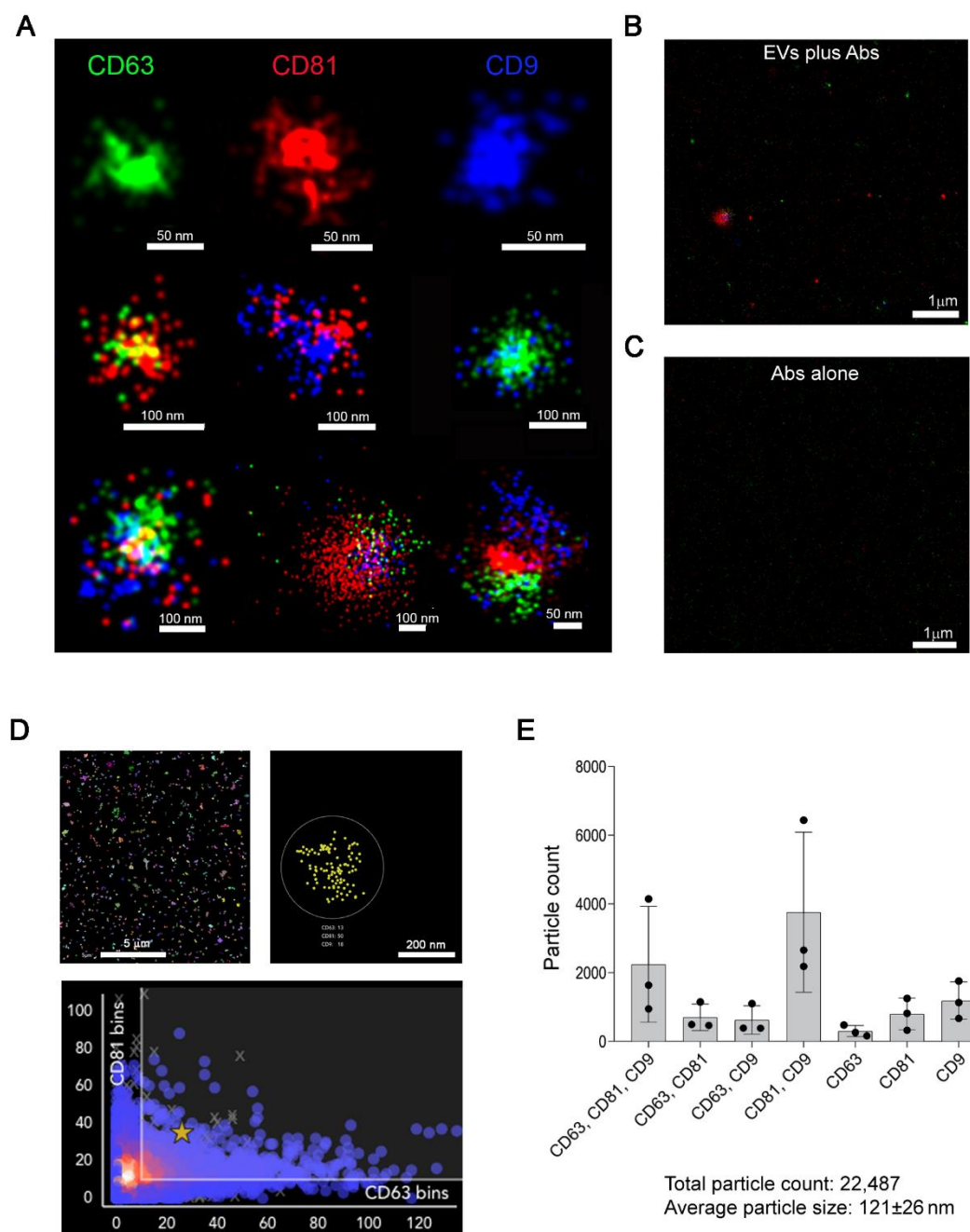
Figure 2. **Super-resolution microscopy analysis of tetraspanins expression in NP-EVs.**
**A)** *Representative super-resolution microscopy images of NP-EVs showing single, double, and triple expression of CD63 (green), CD81 (red), CD9 (blue). The corresponding scale bare is below each EV image.* **B)** *Representative super-resolution images, at low magnification, showing staining with anti-tetraspanin antibodies in the presence of EVs (EVs plus Abs) or* **C)** *in the absence of EVs (Abs alone).* **D)** *Representative clustering strategy of NP-EV analysis showing a large field of view (left panel), a selected cluster (right panel) and a graph (bottom panel) of CD81/CD63 cluster distribution.* **E)** *Clustering analysis of super-resolution microscopy images showing the single, double, and triple positive EV fractions expressing the tetraspanin markers. The analyses were performed in 3 NP-EV preparations using a CODI software; the graph shows the mean ± SD of a cumulative analysis of 10 fields for each preparation.*

18

Comparison of amniotic fluid EVs from normal and preeclamptic pregnancies

EVs were also isolated from term-amniotic fluid of 7 preeclamptic pregnancies (Table 1). The different volumes and EV concentrations in each sample are reported in Supplementary Table 1. No difference in mean EV concentration between NP-EVs and PE-EVs (2.85×10^9 and 2.17×10^9 particles/ml, respectively) was observed, although the relevance of this parameter is limited by the dynamic nature of this biofluid (Underwood, Gilbert and Sherman, 2005). As amniotic fluid contains EVs originating from several sources, a comprehensive analysis of EV surface receptors characterizing several cell types was performed using MACSPlex, a bead-based cytofluorimetric kit able to perform a semiquantitative fluorescent analysis of 39 different EV surface markers. Figure 3A shows the most relevant markers expressed. EVs within the amniotic fluid of both normal and preeclamptic pregnancies highly expressed tetraspanins, as confirmed with the methods shown above. In addition, the typical amniotic fluid marker, CD24 (Keller *et al.*, 2007) and CD133, known to be highly expressed by urine EVs (Dimuccio *et al.*, 2014) were present at a high level in both EV types, indicating the presence of EVs derived from fetal urine. Expression of the embryonic stem and epithelial cell marker CD326 was detected in both samples. Interestingly, a significantly higher expression of the progenitor/mesenchymal marker SSEA-4 and CD105 was detected in PE-EVs (Figure 3A). No expression of leukocyte (CD3, CD4, CD8, CD45, CD56, CD19), endothelial (CD31) or platelet (CD42a and CD49e) markers was observed (data not shown).

ExoView analysis was subsequently used to assess at single-EV level the expression of NP-EV and PE-EV surface markers of interest. After EV affinity binding to tetraspanins, CD105, Tie-2, CD117 (c-kit) and HLA-G expression were evaluated on captured EVs (Figure 3C). The analysis confirmed the presence of HLA-G, as shown by super-resolution microscopy, and revealed the presence of the angiogenic marker Tie-2 and of the stem cell marker CD117 on

19

401   both NP- and PE-EVs. In addition, the analysis confirmed the increased expression of CD105

402   in PE-EVs with respect to NP-EVs (Figure 3C). By simultaneously detecting HLA-G along

403   with the other makers, we were able to assess their co-expression. The analysis showed that

404   the HLA-G expressing EVs displayed similar CD105 and c-kit markers levels, suggesting that

405   the increased CD105 expressing EVs present in PE were not of placental origin (Figure 3D).

406   At variance, Tie-2 levels were significantly lower in placental EVs of PE pregnancies. No

407   differences in tetraspanin levels, used as control, were observed (Supplementary Figure 1B).

408   The increased CD105 expression in PE-EVs with respect to NP-EVs was also confirmed by

409   Western Blot analysis (Supplementary Figure 2).

20
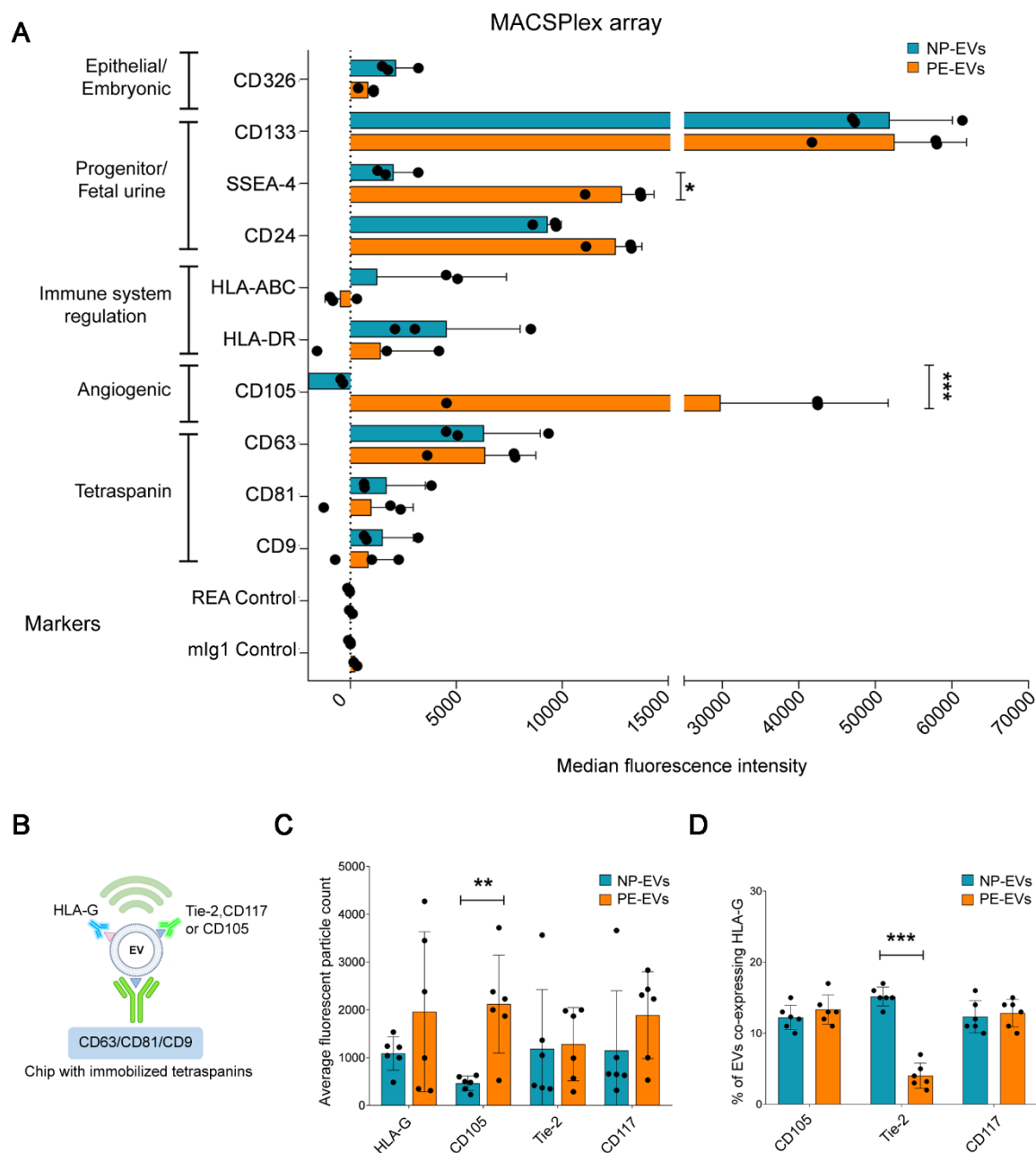
Figure 3. Increased CD105 expression in PE-EVs. A) *MACSPlex analysis showing the median fluorescence intensity of surface markers characteristic of EVs (tetraspanins) or different cell of origin, expressed by NP- and PE-EVs (n=3). Expression of CD105 and SSEA-4 was significantly increased in PE-EVs. 5.8x10^8 EVs were analysed, diluted to a final volume of 120 µl of MACSPlex buffer.* **B)** *Diagram explaining the experimental method behind ExoView technology in relation to the graphs in panel C.* **C and D)** *ExoView analysis of amniotic fluid-derived NP-EVs (n=6) and PE-EVs (n=6).* **C)** *Comparison of the expression of HLA-G, Tie-2, CD105 and CD117 (c-kit) shown as average fluorescent particle count in NP-EVs vs PE-EVs from combined tetraspanins capture of CD63, CD81 and CD9.* **D)** *Normalized expression of HLA-G positive EVs co-expressing other angiogenic (CD105 and Tie-2) and stem cell (CD117) markers. 5.8x10^8 EVs in final volume of 35 µl of buffer were used for all samples. Unpaired Student's t-test: *=P<0.05, * *=P<0.01, ***=P<0.001*

21

422   Finally, we tested the characteristics of EVs derived from cultured term AFSCs, as a possible

423   source of amniotic fluid-EVs (Figure 4). Detection of AFSC-derived EVs captured on

424   tetraspanin coated chips revealed the presence of distinct subpopulations of HLA-G and CD105

425   expressing EVs, being CD105$^+$ EVs the larger fraction. No co-expression of the two markers

426   was observed (Figure 4A and B). Analysis of the HLA-G$^+$ AFSC-EV fraction by MACSPlex

427   analysis confirmed the lack of CD105 expression (Figure 4C and D). These data suggest that

428   the CD105$^+$ EV fraction observed in PE-EVs could possibly derive from cells of fetal or fetal

429   membrane origin, including AFSCs.

430
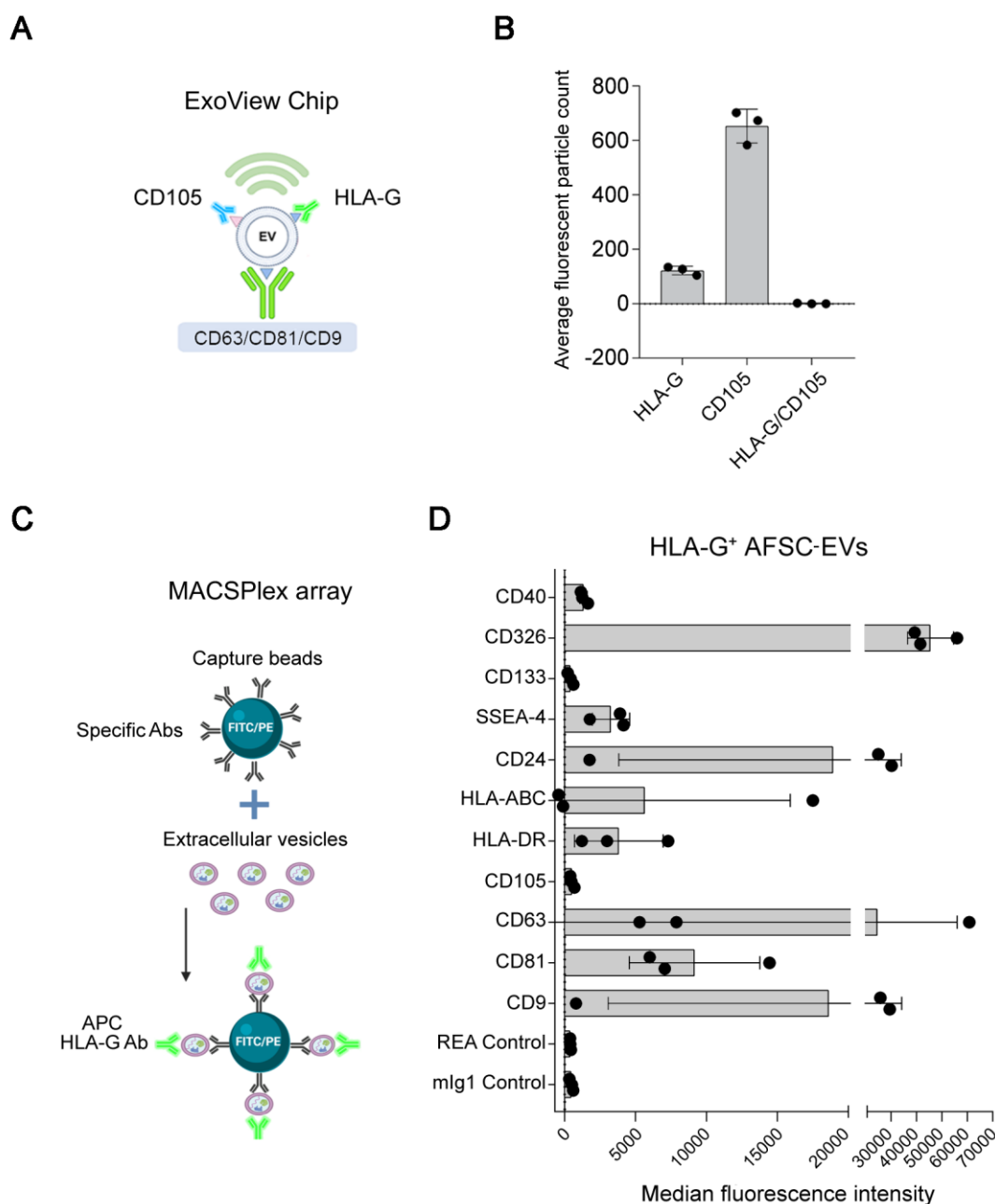
Figure 4. **Characterization of HLA-G-expressing EVs from term AFSCs. A**) *Diagram explaining the experimental method in relation to the graph in panel B.* **B**) *Fluorescent particle count of AFSC-EVs captured on tetraspanin-coated chip analyzed by ExoView, showing expression of HLA-G⁺ and CD105⁺ EVs, but lack of co-expression of the markers.* **C**) *Graphical representation of MASCPlex analyses to characterize HLA-G⁺ AFSC-EVs, using Ab-coated fluorescent beads and APC-labelled anti-HLA-G Ab.* **D**) *The graph shows the median fluorescence intensity of surface markers co-expressed on HLA-G⁺ AFSC-EVs (n=3). AFSC-EVs (5.8x10⁸) were gated for the HLA-G positivity and analysed for the expression of a panel of markers. No expression of CD105 was detected. Illustrations in panels A and C were created with https://biorender.com.*

440

23

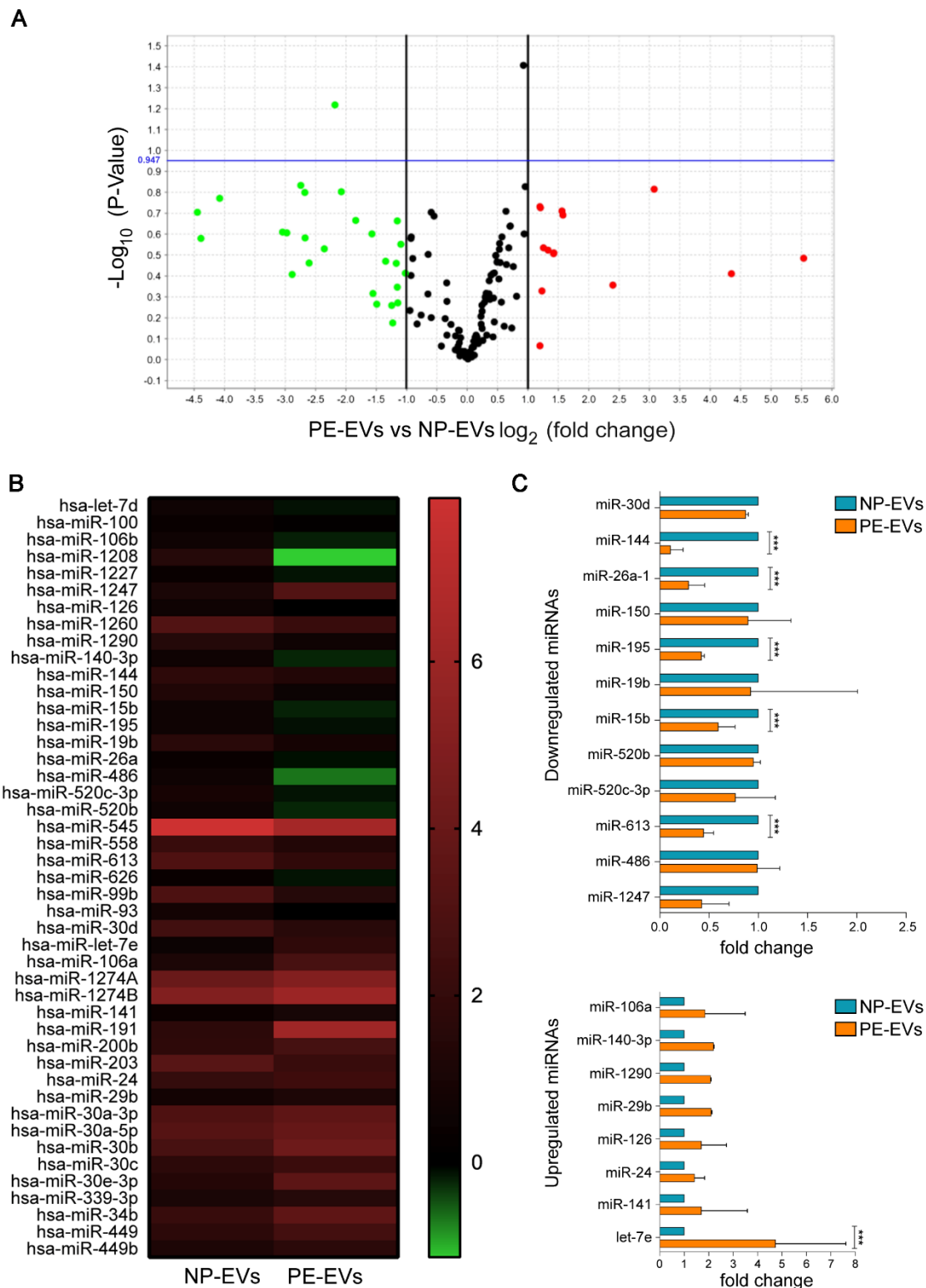441 **Functional characterization of NP-EVs and PE-EVs on angiogenesis**

442 Soluble endoglin is a differentially spliced form of endoglin and is a relevant antiangiogenic

443 factor in PE, acting as a decoy receptor for transforming growth factor beta (TGF-β) (Valluru

444 *et al.*, 2011). To test the angiogenic properties of NP-EVs, PE-EVs, and the possible role of

445 CD105 increased expression on the EV surface, a tube formation assay was performed.

446 Amniotic fluid-derived EVs both from NP and PE, showed a significant reduction in the

447 organization of the HUVEC into capillary-like structures on Matrigel, with respect to the

448 positive control, with the PE-EVs being significantly more effective than NP-EVs in reducing

449 tube formation. To test the relative role of the increased expression level of CD105 on the

450 surface of PE-EVs, TRC-105, an anti-CD105 monoclonal Ab used as an antiangiogenic drug

451 (Brossa, Buono and Bussolati, 2018), was applied. We found that the addition of TRC-105 to

452 PE-EVs, but not to NP-EVs, prior to HUVEC stimulation significantly abolished their

453 inhibitory effect (Figure 5), indicating the role of surface CD105 in angiogenesis reduction.

454

24

A

B
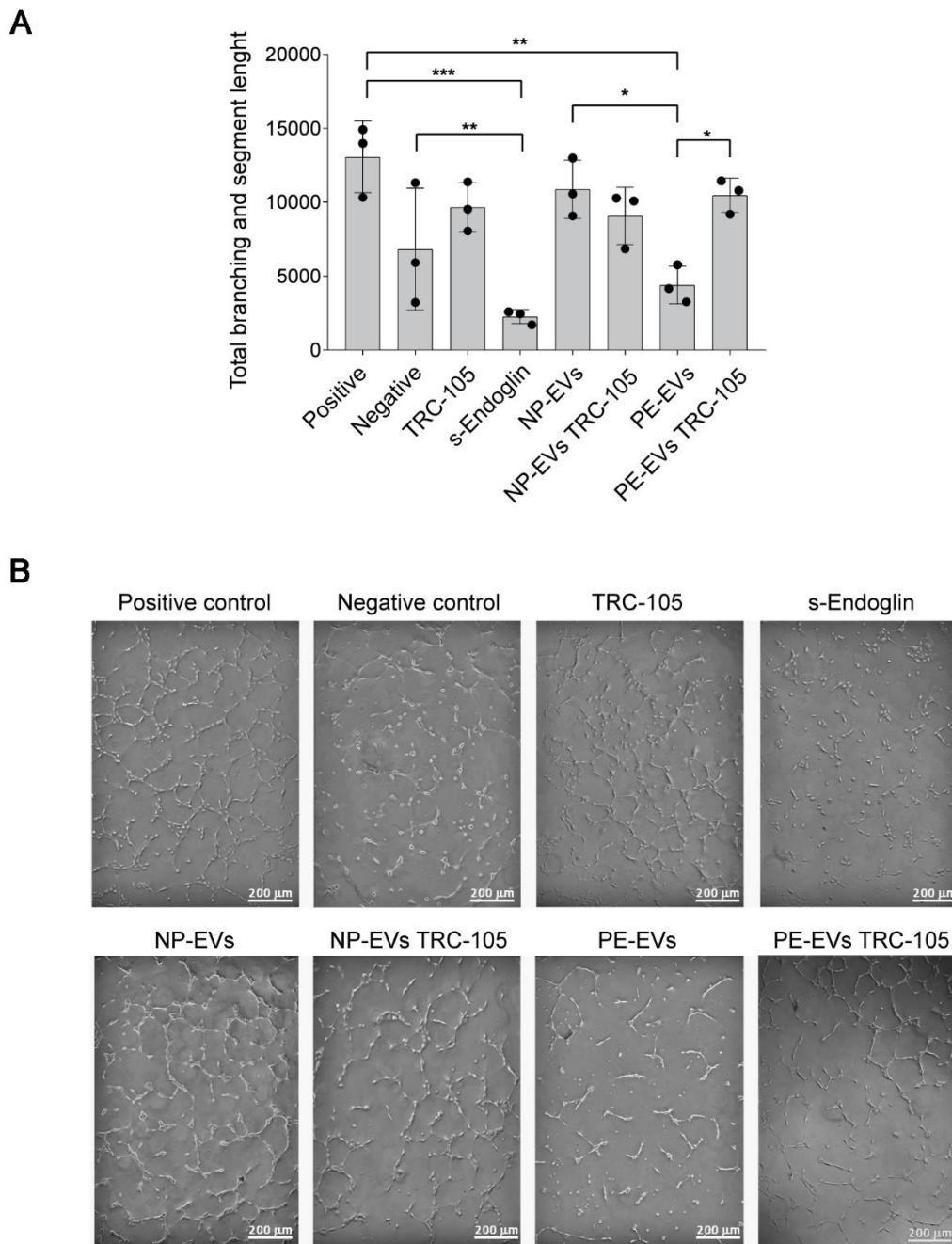
455
456 *Figure 5. Effect of NP-EVs and PE-EVs on tube formation and role of CD105. A) Quantification of*
457 *tube lengths of HUVEC treated with NP-EVs, PE-EVs with or without anti-CD105 Ab (TRC-105) (8*
458 *μg/ml). A concentration of 1000 EVs/cell was used. Positive control: complete EBM medium; negative*
459 *control: EBM medium without FBS. s-Endoglin (100 ng/ml) was used as control for angiogenesis*
460 *inhibition. Statistical analysis was performed using ANOVA with Bonferroni's post-hoc test. *=P<0.05,*
461 ***=P<0.01, ***=P<0.001. B) Representative images of the tube formation assay.*
462

463

464

25

Differential miRNA expression in NP-EVs and PE-EVs

465

466 In order to identify the key regulatory miRNA in amniotic-derived EVs and their possible

467 differential expression in PE-EVs, we performed miRNA arrays on SEC-purified EV

468 preparations from 3 NP and 3 PE amniotic fluids. A large number of miRNAs were present in

469 amniotic fluid-EVs. The 3 sample repeats were combined for ease of interpretation. The raw

470 data can be found at https://fairdomhub.org/projects/244, showing miRNA expression for each

471 individual sample. The top and bottom 10 expressed miRNAs in NP-EVs are shown in

472 Supplementary Table 2. Overall, 46 miRNAs were detected as differentially expressed in PE-

473 EVs vs NP-EVs (Figure 6A and B). The complete list of miRNAs can be found at

474 https://fairdomhub.org/data_files/4182?version=1. In particular, 20 miRNAs of interest were

475 selected for qRT-PCR validation as previously described in EVs, biological fluids or placental

476 tissue from preeclamptic women from literature analysis (Supplementary Table 4). Results

477 confirmed a deregulated trend of the majority of miRNAs in PE-EVs, with let-7e, miR-15b,

478 miR-195,miR-613, miR-26a and miR-144 showing significance (Figure 6C).

Figure 6. MiRNA analysis of NP-EVs and PE-EVs. *A) Volcano plot showing the differential expression of miRNAs derived from NP-EVs vs PE-EVs. **B)** Heatmap showing the miRNAs with the highest fold changes between the samples. **C**) Validation of the deregulated miRNAs, normalized to RNU6 and CTL, as evaluated by qRT-PCR analysis. Data are expressed as mean ± SD of at least three different experiments normalized to CTL and to one, with let-7e, miR-195, miR-613, miR-15b, miR-26a-1, and miR-144, showing significant regulation differences. Unpaired Student's t-test: ***=P<0.001.*

27

486   **Bioinformatic analysis**

487   The search of deregulated miRNA gene targets revealed more than 1000 strong evidence

488   miRNA-gene interactions, involving 667 unique genes, with the vascular endothelial growth

489   factor (VEGF) gene being central in the interactome (Supplementary Figure 3). Further

490   functional enrichment analysis of GO terms and pathways supported the overall miRNA

491   involvement in the regulation of angiogenesis and vascular remodeling (Supplementary Figure

492   4 and 6).

493   Accordingly, the analysis of target tissue and cell specific gene expression profile identified,

494   among the top represented, myoblast, omentum and placenta (Supplementary Figure 5).

495   Finally, analysing for miRNAs acting on a common target and resulting in an increased

496   inhibitory effect *via* triplex analysis, COL22A1, coding for collagen XXII, appeared to be

497   targeted by cooperative miRNAs with the lowest predicted repression (Supplementary Figure

498   6). Further details can be found in the bioinformatic section of supplementary data. The

499   complete list of miRNA gene targets and network enrichment results from EnrichR and BinGo

500   can be found at: https://fairdomhub.org/projects/244.

501

502

28

Discussion

503

504 As reproductive EV research advances, investigation of placenta, surrounding gestational

505 tissues, and amniotic fluid is of profound importance, in order to understand the factors

506 involved in fetal development and maternal health. This paper provides for the first time a deep

507 characterization of EVs present in term amniotic fluid in normal and preeclamptic pregnancies.

508 Using several orthogonal techniques (chip-based platform, cytofluorimetric bead-based

509 multiplex assay and super-resolution microscopy analysis), we show that EVs of term amniotic

510 fluid represent a heterogeneous population of EVs of multiple origins, including placental

511 tissues, fetal urine, and stem cells. Moreover, we identified potential antiangiogenic properties

512 of amniotic fluid-EVs from preeclamptic pregnancies, supported by the specific upregulation

513 of the CD105 surface marker and the deregulation of several angiogenic miRNAs (Figure 7).

514 We here characterized EVs isolated from term amniotic fluid using sub-sequential

515 centrifugation, and we further purified them for the identification of specific surface receptors

516 and miRNA cargo using size-exclusion chromatography to remove contaminating factors

517 possibly present in the amniotic fluid (Monguió-Tortajada *et al.*, 2019; Théry *et al.*, 2018). The

518 characterization of NP-EVs at a single-EV level revealed a highly heterogeneous population of

519 EVs with variable tetraspanins expression. These results are in agreement with those reported

520 by Han and colleagues on colocalization analysis of tetraspanins in EVs derived from different

521 cell lines, showing distinct fractions of single, double or triple co-expressing EVs (Han *et al.,*

522 2021).

523 Moreover, based on surface marker expression as well as miRNA content, we found that EVs

524 within the term amniotic fluid may originate from various sources. Indeed, amniotic fluid-EVs

525 expressing CD24 were mainly derived from fetal urine (Keller *et al.,* 2007). In this study, we

526 confirmed the possible cellular origin of the EVs attributed to fetal urine by expression not only

29

527   of CD24 but also of CD133, which is also considered to be highly present in urinary EVs

528   (Dimuccio *et al*., 2014). Additionally, amniotic fluid-EVs expressed mesenchymal and stem

529   markers, possibly suggesting the origin from CD117^{+} amniotic fluid stem cells (Cananzi, Atala

530   and De Coppi, 2009), amniotic CD105^{+} mesenchymal stem cells (Baghaei *et al*., 2017), and

531   SSEA-4^{+} expressing embryonic stem cells (Noisa *et al.,* 2012). Interestingly, we also showed

532   that a large fraction of amniotic NP-EVs expressed HLA-G, as detected by ExoView and super-

533   resolution microscopy. HLA-G, the distinct HLA isoform involved in maternal tolerance of the

534   fetus, was previously reported to characterize EVs from the placenta *in vitro* or *in vivo* in the

535   maternal circulation (Eunsung Mouradian, 2008; Orozco *et al*., 2009). It is also conceivable

536   that the reported presence of HLA-G within the amniotic fluid could be related to its expression

537   on the EV membrane (McMaster *et al*., 1998). The origin of the HLA-G expressing EVs in the

538   amniotic fluid is unclear. They could possibly directly originate from the amniotic membrane

539   surrounding the fetus and containing the amniotic fluid. Another possible explanation is the

540   passage of trophoblast-derived EVs through the chorion and amnion to reach the amniotic fluid

541   (McMaster *et al*., 1998). The placental origin of amniotic fluid-EVs is also suggested by the

542   analyses of the deregulated miRNA target genes in preeclampsia, showing the most represented

543   cell targets origin from the myoblast, the omentum and the placenta. The placental and stem

544   cell origin of NP-EVs supports their use in regenerative medicine, as recently proposed

545   (Mitrani *et al*., 2021).

546   Proteomic and miRNA profile analysis of amniotic fluid-EVs has been gaining an increasing

547   interest in identifying disease-associated biomarkers and mechanisms (Dixon *et al.*, 2018). In

548   this study, we identified the specific increase in the levels of surface-associated CD105 in PE-

549   EVs, whereas other surface markers showed similar expression levels. Endoglin (CD105) is a

550   co-receptor of TGF-β1 and TGF-β3, highly expressed on the surface of syncytiotrophoblasts

551   and endothelial cells (Valluru *et al*., 2011). An increase in soluble endoglin is a hallmark of

552   preeclampsia (Mutter and Karumanchi, 2008; Schuster *et al*., 2020) and is responsible for

553   endothelial damage by trapping soluble TGF-β molecules (Valluru *et al.*, 2011). We here

554   confirmed the increased CD105 levels through different orthogonal techniques. The use of a

555   CD105-based capture chip allowed us to demonstrate that the increase in CD105 expression

556   was not due to HLA-G expressing placental EVs. The origin of CD105 expressing EVs could

557   be possibly attributed to cells of fetal or fetal membrane origin in the fluid, including AFSCs.

558   Indeed, the analysis of cultured amniotic fluid mesenchymal stromal cells showed that the

559   released EVs were largely CD105$^+$, whereas the HLA-G$^+$ EVs, representing a minor fraction,

560   did not co-express CD105. It would be of interest in future studies to evaluate the CD105/HLA-

561   G co-expression by cells isolated from preeclamptic amniotic fluid.

562
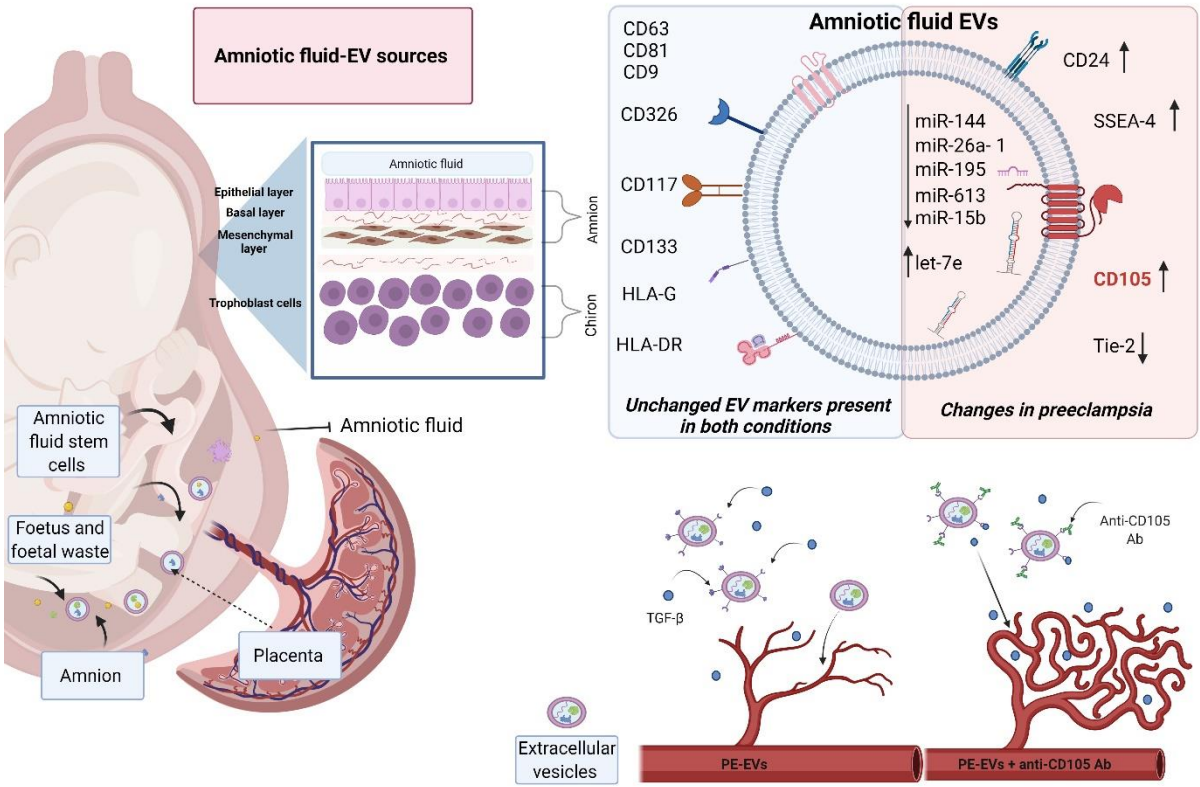
563   ***Figure 7**. **Graphical illustration summarizing the main findings**. The figure shows the multiple*
564   *possible sources of term amniotic fluid-derived EVs and the main changes in PE-EVs. Their*
565   *antiangiogenic properties are supported by the specific upregulation of CD105 surface marker and the*
566   *deregulation of several angiogenic miRNAs. The image was created with https://biorender.com.*

31

567   The increased CD105 level in PE-EVs is in agreement with previous data, showing higher

568   levels of endoglin on EVs produced by placental explants treated with preeclamptic sera

569   (Tannetta *et al.*, 2013) and support the concept that surface receptors expressed by EVs may

570   act as a decoy for soluble factors (Tannetta *et al.*, 2013; Sedrakyan *et al.*, 2017). In analogy,

571   we found that PE-EVs affected angiogenesis *in vitro* and that this effect was abolished when

572   CD105 was blocked by a specific antibody. A slight antiangiogenic effect was also observed

573   for NP-EVs, in parallel with data showing that AFSC-EVs do not promote angiogenesis despite

574   their regenerative effect (Takov *et al.*, 2020). However, this was not prevented by the anti-

575   CD105 antibody, suggesting the involvement of other factors. Previous data showed that

576   administration of human EVs derived from preeclamptic placentas in mice resulted in damage

577   to the vasculature, poor fetal nutrition and promoted endothelial permeability and glomeruli

578   damage (Chang *et al.*, 2018). In particular, the study provided an additional mechanism for the

579   antiangiogenic effect of EVs, related to the presence of soluble endoglin transfer from the EV

580   cargo to endothelial cells (Chang *et al.*, 2018). Our results, showing the antiangiogenic effect

581   of amniotic preeclamptic EVs, highlight a new role for EVs present in the amniotic fluid,

582   possibly acting on both fetal and maternal compartments. Indeed, many reports described feto-

583   placental endothelial dysfunction in preeclampsia, as a detriment to both the mother and the

584   fetus (Escudero *et al*., 2016). It would be of interest to investigate the possible effect of PE-

585   EVs on fetal development.

586   Several miRNAs with relevant roles in placenta development and angiogenesis have been

587   detected in biological fluids and tissues of preeclamptic patients, including specific miRNA

588   sets in the deriving EVs and are considered as a potential biomarker and "fingerprint" of

589   placental dysfunction (Fallen *et al.*, 2018; Gray *et al.*; 2017; Menon *et al.*, 2019; Salomon *et*

590   *al.*, 2017; Ospina-Prieto *et al.*, 2016; Escudero *et al.*, 2016; Cronqvist *et al.*, 2017). We here

591   identified 46 miRNAs deregulated in amniotic fluid-derived PE-EVs, and we confirmed a

32

592   differential expression in 6 miRNAs, involved in trophoblast proliferation and invasion (let-7

593   and miR-613), as well as in the modulation of placental function (miR-15, miR-26a) and

594   angiogenesis (miR-195, and miR-144) (Cross *et al.,* 2015, Hu *et al.,* 2009, Bai *et al.,* 2012

595   Guan *et al.,* 2016 Choi *et al.,* 2013 Li *et al.,* 2013). Interestingly, although these miRNAs did

596   not overlap with the EV miRNA profile alterations described in maternal circulation (Fallen *et*

597   *al.*, 2018; Gray *et al.*; 2017; Menon *et al.*, 2019; Salomon *et al.*, 2017), the majority (let-7,

598   miR-15b, miR-195, and miR-26a-1) have been reported to be modulated in placental tissue of

599   preeclamptic patients (Cross *et al.,* 2015; Mayor-Lynn *et al.,* 2011; Hu *et al.*, 2009; Bai *et al.*,

600   2012; Choi *et al.,* 2013). This underlines a differential profile of amniotic fluid-EVs from those

601   in the maternal circulation, and may further support their origin from placental deriving cells.

602   These differentially expressed miRNAs may target genes involved in various functions,

603   including development and angiogenesis, and are tightly involved in VEGF regulation and

604   vascular remodeling. Indeed, deregulated pathways associated with angiogenesis, invasion and

605   inflammation have been previously reported by target interaction analysis of miRNA content

606   carried by preeclamptic maternal blood (Pillay *et al*., 2019, Salomon *et al.*, 2017).

607   In conclusion, our study characterizes at single-EV level, EVs present in the amniotic fluid, an

608   interesting biofluid with a possible relevance for therapeutic application. Amniotic fluid-

609   derived EVs showed a heterogeneous origin, expressing markers of fetal and placental cells.

610   We highlight the differential expression of antiangiogenic factors in normal and preeclamptic

611   amniotic fluid-derived EVs, both at surface and cargo level. These characteristics may reflect

612   the hypoxic and antiangiogenic general status of preeclampsia and could possibly play a role

613   by affecting the developing fetus or the surrounding fetal membranes. Finally, EVs within the

614   amniotic fluid could potentially be used as a diagnostic test if investigated at earlier stages of

615   pregnancy.

616

625

626

627

References:

Amaral, L. M. *et al.* (2015) 'Preeclampsia: Long-term consequences for vascular health', *Vascular Health and Risk Management*, 11, pp. 403–415. doi: 10.2147/VHRM.S64798.

Baghaei, K. *et al.* (2017) 'Isolation, differentiation, and characterization of mesenchymal stem cells from human bone marrow', *Gastroenterology and Hepatology from Bed to Bench*, 10(3), pp. 208–213. doi: 10.22037/ghfbb.v0i0.1089.

Bai, Y. *et al.* (2012) 'Downregulated miR-195 detected in Preeclamptic Placenta affects trophoblast cell invasion via modulating ActRIIA expression', *PLoS ONE*, 7(6). doi: 10.1371/journal.pone.0038875.

Balbi, C. *et al.* (2017) 'First characterization of human amniotic fluid stem cell extracellular vesicles as a powerful paracrine tool endowed with regenerative potential', *Stem Cells Translational Medicine*, 6(5), pp. 1340–1355. doi: 10.1002/sctm.16-0297.

Bindea, G. *et al.* (2009) 'ClueGO: A Cytoscape plugin to decipher functionally grouped gene ontology and pathway annotation networks', *Bioinformatics*, 25(8), pp. 1091–1093. doi: 10.1093/bioinformatics/btp101.

Brossa, A., Buono, L. and Bussolati, B. (2018) 'Effect of the monoclonal antibody TRC105 in combination with Sunitinib on renal tumor derived endothelial cells', *Oncotarget*, 9(32), pp. 22680–22692. doi: 10.18632/oncotarget.25206.

Brown, M. A. *et al.* (2018) 'Hypertensive disorders of pregnancy: ISSHP classification, diagnosis, and management recommendations for international practice', *Hypertension*, 72(1), pp. 24–43. doi: 10.1161/HYPERTENSIONAHA.117.10803.

Cananzi, M., Atala, A. and De Coppi, P. (2009) 'Stem cells derived from amniotic fluid: New potentials in regenerative medicine', *Reproductive BioMedicine Online*, 18, pp. 17–27. doi: 10.1016/S1472-6483(10)60111-3.

Chang, X. *et al.* (2018) 'Exosomes from women with preeclampsia induced vascular dysfunction by delivering sFLT (soluble fms-like tyrosine kinase)-1 and SENG (soluble endoglin) to endothelial cells', *Hypertension*, 72(6), pp. 1381–1390. doi: 10.1161/HYPERTENSIONAHA.118.11706.

Chen, E. Y. *et al.* (2013) 'Enrichr: Interactive and collaborative HTML5 gene list enrichment analysis tool', *BMC Bioinformatics*, 14. doi: 10.1186/1471-2105-14-128.

Choi, S. Y. *et al.* (2013) 'MicroRNA expression profiles in placenta with severe preeclampsia using a PNA-based microarray', *Placenta*, 34(9), pp. 799–804. doi: 10.1016/j.placenta.2013.06.006.

Cronqvist, T. *et al.* (2017) 'Syncytiotrophoblast derived extracellular vesicles transfer functional placental miRNAs to primary human endothelial cells', *Scientific Reports*, 7(1), pp. 1–14. doi: 10.1038/s41598-017-04468-0.

Cross, C. E. *et al.* (2015) 'Oxidative Stress Alters miRNA and Gene Expression Profiles in Villous First Trimester Trophoblasts', *BioMed Research International*, 2015. doi:

35

666   10.1155/2015/257090.

667   Dimuccio, V. *et al.* (2014) 'Urinary CD133+ extracellular vesicles are decreased in kidney
668   transplanted patients with slow graft function and vascular damage', *PLoS ONE*, 9(8). doi:
669   10.1371/journal.pone.0104490.

670   Dixon, C. L. *et al.* (2018) 'Amniotic fluid exosome proteomic profile exhibits unique
671   pathways of term and preterm labor', *Endocrinology*, 159(5), pp. 2229–2240. doi:
672   10.1210/en.2018-00073.

673   Duley, L. (2009) 'The global impact of pre-eclampsia and eclampsia.', *Seminars in*
674   *perinatology*, 33(3), pp. 130–7. doi: 10.1053/j.semperi.2009.02.010.

675   Escudero, C. A. *et al.* (2016) 'Role of extracellular vesicles and microRNAs on dysfunctional
676   angiogenesis during preeclamptic pregnancies', *Frontiers in Physiology*, 7(MAR), pp. 1–17.
677   doi: 10.3389/fphys.2016.00098.

678   Eunsung Mouradian, M. M. (2008) 'Immunomodulatory molecules are released from the first
679   trimester and term placenta via exosomes', *Bone*, 23(1), pp. 1–7. doi:
680   10.1016/j.placenta.2012.10.005.Immunomodulatory.

681   Fallen, S. *et al.* (2018) 'Extracellular vesicle RNAs reflect placenta dysfunction and are a
682   biomarker source for preterm labour', *Journal of Cellular and Molecular Medicine*, 22(5), pp.
683   2760–2773. doi: 10.1111/jcmm.13570.

684   Gebara, N. *et al.* (2021) 'Angiogenic properties of placenta-derived extracellular vesicles in
685   normal pregnancy and in preeclampsia', *International Journal of Molecular Sciences*, 22(10).
686   doi: 10.3390/ijms22105402.

687   Gray, C. *et al.* (2017) 'Maternal plasma miRNAs as biomarkers during mid-pregnancy to
688   predict later spontaneous preterm birth: A pilot study', *Scientific Reports*, 7(1), pp. 1–7. doi:
689   10.1038/s41598-017-00713-8.

690   Han, C. *et al.* (2021) 'Single-vesicle imaging and colocalization analysis for tetraspanin
691   profiling of individual extracellular vesicles', *Journal of Extracellular Vesicles*, 10(3). doi:
692   10.1002/jev2.12047.

693   Hromadnikova, I. *et al.* (2015) 'Cardiovascular and cerebrovascular disease associated
694   microRNAS are dysregulated in placental tissues affected with gestational hypertension,
695   preeclampsia and intrauterine growth restriction', *PLoS ONE*, 10(9), pp. 1–27. doi:
696   10.1371/journal.pone.0138383.

697   Hu, Y. *et al.* (2009) 'Differential expression of microRNAs in the placentae of Chinese
698   patients with severe pre-eclampsia', *Clinical Chemistry and Laboratory Medicine*, 47(8), pp.
699   923–929. doi: 10.1515/CCLM.2009.228.

700   Huang, H. Y. *et al.* (2020) 'MiRTarBase 2020: Updates to the experimentally validated
701   microRNA-target interaction database', *Nucleic Acids Research*, 48(D1), pp. D148–D154.
702   doi: 10.1093/nar/gkz896.

703   Iampietro, C. *et al.* (2020) 'Full-Term Human Amniotic Fluid Mesenchymal Stem Cells Show
704   Nephroprotective Effect In An Acute Kidney Injury Model', *Journal of Stem Cells Research,*

705   *Development & Therapy*, 6(3), pp. 1–8. doi: 10.24966/srdt-2060/100041.

706   Jankovičová, J. *et al.* (2020) 'Tetraspanins, more than markers of extracellular vesicles in
707   reproduction', *International Journal of Molecular Sciences*, 21(20), pp. 1–30. doi:
708   10.3390/ijms21207568.

709   Jassal, B. *et al.* (2020) 'The reactome pathway knowledgebase', *Nucleic Acids Research*,
710   48(D1), pp. D498–D503. doi: 10.1093/nar/gkz1031.

711   Kaufmann, P., Black, S. and Huppertz, B. (2003) 'Endovascular trophoblast invasion:
712   Implications for the pathogenesis of intrauterine growth retardation and preeclampsia',
713   *Biology of Reproduction*, 69(1), pp. 1–7. doi: 10.1095/biolreprod.102.014977.

714   Keller, S. *et al.* (2007) 'CD24 is a marker of exosomes secreted into urine and amniotic fluid',
715   *Kidney International*, 72(9), pp. 1095–1102. doi: 10.1038/sj.ki.5002486.

716   Lai, X. *et al.* (2012) 'Computational analysis of target hub gene repression regulated by
717   multiple and cooperative miRNAs', *Nucleic Acids Research*, 40(18), pp. 8818–8834. doi:
718   10.1093/nar/gks657.

719   Maere, S., Heymans, K. and Kuiper, M. (2005) 'BiNGO: a Cytoscape plugin to assess
720   overrepresentation of Gene Ontology categories in Biological Networks', *Bioinformatics*,
721   21(16), pp. 3448–3449. doi: 10.1093/bioinformatics/bti551.

722   Martin, A. *et al.* (2010) 'BisoGenet: A new tool for gene network building, visualization and
723   analysis', *BMC Bioinformatics*, 11. doi: 10.1186/1471-2105-11-91.

724   Mayor-Lynn, K. *et al.* (2011) 'Expression profile of microRNAs and mRNAs in human
725   placentas from pregnancies complicated by preeclampsia and preterm labor', *Reproductive
726   Sciences*, 18(1), pp. 46–56. doi: 10.1177/1933719110374115.

727   McMaster, M. *et al.* (1998) 'HLA-G isoforms produced by placental cytotrophoblasts and
728   found in amniotic fluid are due to unusual glycosylation.', *Journal of immunology*, 160(12),
729   pp. 5922–8. Available at: http://www.ncbi.nlm.nih.gov/pubmed/9637505.

730   Menon, R. *et al.* (2019) 'Circulating exosomal miRNA profile during term and preterm birth
731   pregnancies: A longitudinal study', *Endocrinology*, 160(2), pp. 249–275. doi:
732   10.1210/en.2018-00836.

733   Mitrani, M. I. *et al.* (2021) 'Case Report: Administration of Amniotic Fluid-Derived
734   Nanoparticles in Three Severely Ill COVID-19 Patients', *Frontiers in Medicine*, 8(March),
735   pp. 1–8. doi: 10.3389/fmed.2021.583842.

736   Monguió-Tortajada, M. *et al.* (2019) 'Extracellular vesicle isolation methods: rising impact of
737   size-exclusion chromatography', *Cellular and Molecular Life Sciences*, 76(12), pp. 2369–
738   2382. doi: 10.1007/s00018-019-03071-y.

739   Montis C., *et al.* (2017). 'Size distribution of extracellular vesicles by optical correlation
740   techniques', *Colloids Surf B Biointerfaces,* 158:331-338. doi: 10.1016/j.colsurfb.2017.06.047.

741   Mutter, W. P. and Karumanchi, S. A. (2008) 'Molecular mechanisms of preeclampsia',
742   *Microvascular Research*, 75(1), pp. 1–8. doi: 10.1016/j.mvr.2007.04.009.

743 Nair, S. *et al.* (2021) 'Placenta-Derived Exosomes and Syncytiotrophoblast Microparticles
744 and their Role in Human Reproduction: Immune Modulation for Pregnancy Success',
745 *Seminars in Immunopathology*, 72(5), pp. 440–457. doi: 10.1111/aji.12311.

746 Nair, S. and Salomon, C. (2018) 'Extracellular vesicles and their immunomodulatory
747 functions in pregnancy', *Seminars in Immunopathology*, 40(5), pp. 425–437. doi:
748 10.1007/s00281-018-0680-2.

749 Noisa, P. *et al.* (2012) 'Identification and Characterisation of the Early Differentiating Cells
750 in Neural Differentiation of Human Embryonic Stem Cells', *PLoS ONE*, 7(5). doi:
751 10.1371/journal.pone.0037129.

752 Ogata, H. *et al.* (1999) 'KEGG: Kyoto encyclopedia of genes and genomes', *Nucleic Acids
753 Research*, pp. 29–34. doi: 10.1093/nar/27.1.29.

754 Orozco, A. F. *et al.* (2009) 'Placental Release of Distinct DNA-associated Micro-particles
755 into Maternal Circulation: Reflective of Gestation Time and Preeclampsia', *Placenta*, 30(10),
756 pp. 891–897. doi: 10.1016/j.placenta.2009.06.012.

757 Ospina-Prieto, S. *et al.* (2016) 'MicroRNA-141 is upregulated in preeclamptic placentae and
758 regulates trophoblast invasion and intercellular communication', *Translational Research*,
759 172(March), pp. 61–72. doi: 10.1016/j.trsl.2016.02.012.

760 Pillay, P. *et al.* (2019) 'Exosomal microRNA profiling in early and late onset preeclamptic
761 pregnant women reflects pathophysiology', *International Journal of Nanomedicine*, 14, pp.
762 5637–5657. doi: 10.2147/IJN.S208865.

763 Roubelakis, M. G., Trohatou, O. and Anagnou, N. P. (2012) 'Amniotic fluid and amniotic
764 membrane stem cells: Marker discovery', *Stem Cells International*. doi:
765 10.1155/2012/107836.

766 Rouillard, A. D. *et al.* (2016) 'The harmonizome: a collection of processed datasets gathered
767 to serve and mine knowledge about genes and proteins', *Database : the journal of biological
768 databases and curation*. doi: 10.1093/database/baw100.

769 Salomon, C. *et al.* (2017) 'Placental exosomes as early biomarker of preeclampsia: Potential
770 role of exosomalmicrornas across gestation', *Journal of Clinical Endocrinology and
771 Metabolism*, 102(9), pp. 3182–3194. doi: 10.1210/jc.2017-00672.

772 Schuster, J. *et al.* (2020) 'Placental extracellular vesicles and pre-eclampsia', *American
773 Journal of Reproductive Immunology*, pp. 0–3. doi: 10.1111/aji.13297.

774 Sedrakyan, S. *et al.* (2017) 'Amniotic fluid stem cell-derived vesicles protect from VEGF-
775 induced endothelial damage', *Scientific Reports*, 7(1), pp. 1–12. doi: 10.1038/s41598-017-
776 17061-2.

777 Shannon, P. *et al.* (2003) 'Cytoscape: A software Environment for integrated models of
778 biomolecular interaction networks', *Genome Research*, 13(11), pp. 2498–2504. doi:
779 10.1101/gr.1239303.

780 Skovronova, R. et al. (2021) 'Surface marker expression in small and medium/large
781 mesenchymal stromal cell-derived extracellular vesicles in naïve or apoptotic condition using
782 orthogonal techniques', Cells, 10 (11)(2948). doi.org/10.3390/cells10112948.

783 Staff, A. C. *et al.* (2007) 'Circulating concentrations of soluble endoglin (CD105) in fetal and
784 maternal serum and in amniotic fluid in preeclampsia', *American Journal of Obstetrics and*
785 *Gynecology*, 197(2), pp. 176.e1-176.e6. doi: 10.1016/j.ajog.2007.03.036.

786 Takov, K. *et al.* (2020) 'Small extracellular vesicles secreted from human amniotic fluid
787 mesenchymal stromal cells possess cardioprotective and promigratory potential', *Basic*
788 *Research in Cardiology*, 115(3), pp. 1–22. doi: 10.1007/s00395-020-0785-3.

789 Tannetta, D. S. *et al.* (2013) 'Characterisation of Syncytiotrophoblast Vesicles in Normal
790 Pregnancy and Pre-Eclampsia: Expression of Flt-1 and Endoglin', *PLoS ONE*, 8(2), pp. 1–29.
791 doi: 10.1371/journal.pone.0056754.

792 Théry, C. *et al.* (2018) 'Minimal information for studies of extracellular vesicles 2018
793 (MISEV2018): a position statement of the International Society for Extracellular Vesicles
794 and update of the MISEV2014 guidelines', *Journal of Extracellular Vesicles*, 7(1). doi:
795 10.1080/20013078.2018.1535750.

796 Tong, Z. *et al.* (2019) 'TransmiR v2.0: An updated transcription factor-microRNA regulation
797 database', *Nucleic Acids Research*, 47(D1), pp. D253–D258. doi: 10.1093/nar/gky1023.

798 Underwood, M. A., Gilbert, W. M. and Sherman, M. P. (2005) 'Amniotic fluid: Not just fetal
799 urine anymore', *Journal of Perinatology*, 25(5), pp. 341–348. doi: 10.1038/sj.jp.7211290.

800 Valluru, M. *et al.* (2011) 'Transforming growth factor-β and endoglin signaling orchestrate
801 wound healing', *Frontiers in Physiology*, 2 NOV, pp. 1–12. doi: 10.3389/fphys.2011.00089.

802